THE JOURNAL OF PHYSICAL CHEMISTRY Letters

Letter

pubs.acs.org/JPCL

Intrinsic Piezoelectricity in Two-Dimensional Materials

Karel-Alexander N. Duerloo,[†] Mitchell T. Ong,[†] and Evan J. Reed*

Department of Materials Science and Engineering, Stanford University, Stanford, California 94305, United States

ABSTRACT: We discovered that many of the commonly studied two-dimensional monolayer transition metal dichalcogenide (TMDC) nanoscale materials are piezoelectric, unlike their bulk parent crystals. On the macroscopic scale, piezoelectricity is widely used to achieve robust electromechanical coupling in a rich variety of sensors and actuators. Remarkably, our density-functional theory calculations of the piezoelectric coefficients of monolayer BN, MoS_2, $MoSe_2$, $MoTe_2$, WS_2, WSe_2, and WTe_2 reveal that some of these materials exhibit *stronger* piezoelectric coupling than traditionally employed bulk wurtzite structures. We find that the piezoelectric coefficients span more than 1 order of magnitude, and exhibit monotonic periodic trends. The discovery of this property in many two-dimensional materials enables active sensing, actuating, and new electronic components for *nanoscale* devices based on the familiar piezoelectric effect.

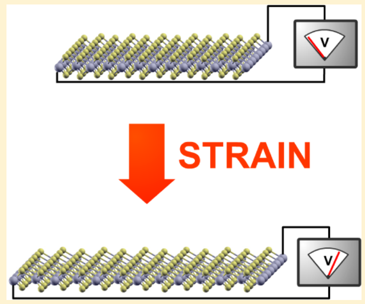

SECTION: Physical Processes in Nanomaterials and Nanostructures

Nanoelectromechanical systems (NEMS) and nanoscale electronics are the final frontier in the push for miniaturization that has been among the dominant themes of technological progress for over 50 years. Enabled by increasingly mature fabrication techniques, low-dimensional materials including nanoparticles, nanotubes, and (near-)atomically thin sheets have emerged as the key components for the next generation of "active nanostructure" NEMS devices including radios,[1] switches,[2−4] tweezers,[5] as well as mass,[6] gas,[7] pressure,[8,9] and displacement sensors.[10] The traditional field effect transistor paradigm has also been extended to nanotubes,[11] graphene,[12] and monolayer MoS_2.[13]

All of the NEMS devices mentioned require some type of static or dynamic mechanical displacement that is electrically sensed, dynamically controlled, or both. Piezoelectric materials have historically been used in many applications requiring electromechanical coupling, and nanoscale devices also stand to gain additional capabilities, simplicity, and autonomous operation through integration of piezoelectric materials. For instance, recent experimental work utilizes piezoelectric micro- or nanowires as piezo-phototronic facilitators for light emission[14] or as the active component of efficient nanogenerators that convert mechanical energy into electricity.[15,16] Piezoelectricity may also be used to generate charge carriers[17] or construct relays[18] in an electronics context. In a rapidly emerging field termed (nano)piezotronics, the controllable charges and electric fields generated by piezoelectrics have been used in several prototype devices such as field effect transistors, piezoelectric-gated diodes, and sensors.[19]

Given these bright prospects for piezoelectricity as an enabler of nanoscale technology along with the explosive advances in fabrication methods, it becomes natural to inquire whether atomically thin sheet materials such as graphene can also be used as piezoelectric building blocks. Recently, we and other researchers have predicted using computational models that graphene can be rendered piezoelectric through adatom adsorption[20] or introduction of specific in-plane defects,[21] paving the way to a strong miniaturization and site-specific engineering of familiar piezoelectric technology using graphene. We now report that a family of widely studied atomically thin sheet materials are in fact *intrinsically* piezoelectric, elucidating an entirely new arsenal of "out of the box" active components for NEMS and piezotronics.

Despite the fact that fullerenes and graphene have made carbon allotropes the most studied of all nanomaterials, graphite is by no means the only layered parent crystal that is amenable to isolation of monolayer sheets. Currently, the most prominent of these other parent crystals are hexagonal boron nitride (h-BN or 2H-BN)[22] and a family of trigonal-prismatically coordinated transition metal dichalcogenide (TMDC) crystals. In keeping with prior literature, we refer to these crystals as 2H-TMDCs, where the 2H prefix is Ramsdell notation for the bulk stacking sequence (two-layer periodic) and the unit cell's basal plane shape (hexagonal).[23] These crystals include, but are not limited to, MoS_2 (monolayers first isolated in 1986),[22,24] WS_2,[25,26] and $NbSe_2$.[22,26] When viewed from the top, the 2H structure of the above materials is a honeycomb structure where adjacent sites are occupied by two alternating species (Figure 1a,b). The difference between h-BN and the 2H-TMDC monolayer structure is that h-BN is atomically thin (Figure 1c), whereas one 2H-TMDC monolayer sublattice contains two chalcogenide atoms at $z = h$ and $z = -h$, and the other sublattice contains a transition metal at $z = 0$ (Figure 1d).

For a material to be piezoelectric, it must not be centrosymmetric (i.e., possess a point through which a spatial inversion leaves the structure invariant).[27] Due to their experimentally observed antiparallel stacking sequence, the

Received: August 22, 2012
Accepted: September 17, 2012
Published: September 17, 2012

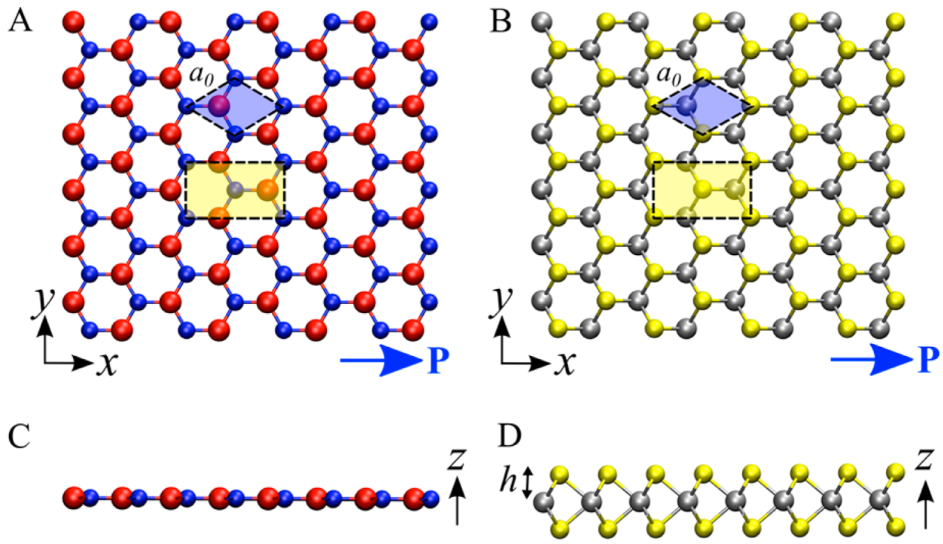

Figure 1. Monolayer top view geometry of (a) boron nitride (h-BN) and (b) trigonal prismatic molybdenum disulfide (2H-MoS_2) where B atoms are red, N atoms are blue, Mo (transition metal) atoms are silver, and S (chalcogenide) atoms are yellow. The axes and direction of piezoelectric polarization are labeled, and the hexagonal primitive cell is highlighted in blue. The orthorhombic unit cell used in the DFT simulations is labeled in yellow. (c) Side view of the atomically thin h-BN monolayer. (d) Side view of the 2H-MoS_2 monolayer, showing out-of-plane structure.

Table 1. Bulk Experimental Lattice Constant a_0, Calculated Monolayer Lattice Constant a_0, Monolayer Chalcogenide Height h, and Monolayer Electronic Band Gap E_{gap} of Different 2D Materials Calculated Using DFT/GGA[a]

material	bulk a_0 (Å)	a_0 (Å) calc.	h (Å) calc.	E_{gap} (eV) calc.	pseudopotentials
h-BN	2.50[28]	2.51	---	4.68	Vanderbilt (n-B)
2H-MoS_2	3.16[29]	3.19	1.57	1.67	PAW (sp-n-Mo, n-S)
2H-$MoSe_2$	3.29[29]	3.33	1.67	1.43	PAW (sp-n-Mo, n-Se)
2H-$MoTe_2$	3.52[29]	3.59	1.82	1.05	norm-conserving[32]
2H-WS_2	3.15[29]	3.19	1.57	1.81	Vanderbilt (n-W)
2H-WSe_2	3.29[29]	3.32	1.67	1.53	Vanderbilt (n-W)
2H-WTe_2	---	3.56	1.82	1.05	norm-conserving[32]
2H-$NbSe_2$	3.45[29]	3.47	1.68	Metallic	Vanderbilt (sp-n-Nb)
2H-$TaSe_2$	3.43[29]	3.47	1.67	Metallic	Vanderbilt (sp-n-Ta)

[a]The atomic pseudopotentials used to simulate the ions include Vanderbilt (ultrasoft), norm-conserving, and projector augmented-wave (PAW) types. Some pseudopotentials include a nonlinear core (n), an s&p-semicore (sp), or d-semicore (d) corrections.

bulk stacked-layer h-BN and 2H-TMDC crystals *are* centrosymmetric.[28,29] At first glance, the presence of centrosymmetry makes these crystals a seemingly fruitless place to look for piezoelectricity. However, it can be seen from Figure 1 that a *single* h-BN or 2H-TMDC monolayer *does not* have an inversion center. Lack of centrosymmetry has the mathematical consequence that all odd-rank tensor properties, including the third-rank piezoelectric tensor, may be nonzero.[27] Hence, a noncentrosymmetric crystal that is found to be electrically insulating is a candidate piezoelectric, regardless of whether it is a one-, two- or three-dimensional structure. This is also the case, for example, in BN nanotubes.[30] The exciting prospect of intrinsically piezoelectric monolayer materials and their potential ramifications for technology in the nanoscale regime has prompted us to *quantitatively* map the piezoelectric and elastic properties of a collection of candidate materials.

We use density functional theory (DFT) at the generalized gradient approximation (GGA) level of theory to calculate the piezoelectric and elastic stiffness coefficients. Piezoelectric properties are associated with ground electronic state changes in polarization, for which DFT generally provides a reasonable description. For example, prior work on the piezoelectric properties of GaN shows agreement with experimental measurements to within approximately 20%.[31] We use the nonprimitive orthorhombic unit cells shown in Figure 1 as the computational unit cell for all calculations. The hexagonal lattice constant a_0 and atomic positions were allowed to relax subject to zero pressure following the convergence criteria listed in the Computational Methods section.

The optimized geometries and calculated band gap energies of h-BN and several 2H-TMDCs are summarized in Table 1. Note that BN, MoS_2, $MoSe_2$, $MoTe_2$, WS_2, $NbSe_2$, and $TaSe_2$ have been experimentally isolated in monolayer form.[26,33] We find $NbSe_2$ and $TaSe_2$ to be metallic and hence not piezoelectric. The monolayer 2H-TMDCs containing Mo or W are found to be insulating. The semilocal DFT-calculated monolayer MoS_2 band gap of 1.67 eV is in reasonable agreement with the experimental value of 1.9 eV.[34] We find the lattice parameters a_0 and h to be correlated primarily to the chalcogenide present in the 2H-TMDC monolayers and largely independent of the transition metal atom type.

It should be stressed that 2H is just one of the possible TMDC structures that are experimentally stable or metastable. For example, monolayers of MoS_2, WS_2, and $MoSe_2$ obtained through water-based lithium intercalation are reported to exhibit a distorted octahedral structure.[35,36] Other authors report using a different solution-based process[26] and mechanical exfoliation[37] to isolate MoS_2 monolayers exhibiting Raman spectra consistent with the 2H structure. Bulk MoS_2, $MoSe_2$, $MoTe_2$, WS_2, and WSe_2 have all been observed in trigonal prismatic (2H) form,[29] but bulk $MoTe_2$ has also been observed as a distorted octahedral structure.[38] The dominant structure of bulk WTe_2 is distorted octahedral.[38] Piezoelectric properties of the metastable 2H form of WTe_2 are still studied in this letter for the purpose of direct comparison with the other structures.

Motivated by the overall scarcity of experimental structural information on monolayers, Table 2 lists our DFT calculations

Table 2. Calculated Differences in Ground-State Energy Per Formula Unit for the Octahedral and Distorted-Octahedral Structures, Referenced to the Trigonal Prismatic 2H Structure of the Studied TMDC Insulators[a]

material	octahedral (eV)	dist. octahedral (eV)
MoS_2		0.55
$MoSe_2$		0.33
$MoTe_2$		0.10
WS_2	0.92	0.54
WSe_2	0.78	0.30
WTe_2	0.57	−0.14

[a]Structural optimization of octahedral Mo-containing monolayers resulted in the distorted octahedral structure. Structures are surrounded by vacuum (i.e. freely suspended).

of the relative energy differences for the 2H, octahedrally coordinated (i.e., The PtS_2 structure),[29] and distorted octahedral monolayer structures of TMDCs in vacuum. The trigonal prismatic 2H structure is found to be lowest in energy for all materials except WTe_2, where the distorted octahedral structure is found to be lowest in energy. We find that the distorted octahedral structures are metallic, ruling out in-plane piezoelectricity.

In order to obtain the elastic stiffness coefficients of the candidate piezoelectrics, the total energy per unit area $u(\varepsilon_{11},\varepsilon_{22})$ is calculated on a 7 × 7 grid with strain components ranging from −0.006 to 0.006 in steps of 0.002. Atomic positions are relaxed at each strain state to generate the so-called relaxed-ion coefficients that are expected to be experimentally observable. Another calculation is performed at each strain state with scaled atomic positions (i.e., no atomic relaxation) to yield so-called clamped-ion coefficients. Planar elastic stiffness coefficients for both cases C_{11} and C_{12} are obtained by fitting the obtained $u(\varepsilon_{11},\varepsilon_{22})$ to eq 1:

$$u(\varepsilon_{11}, \varepsilon_{22}) = \frac{1}{2}C_{11}(\varepsilon_{11}^2 + \varepsilon_{22}^2) + C_{12}\varepsilon_{11}\varepsilon_{22} \tag{1}$$

Clamped- and relaxed-ion elastic coefficients are summarized in Table 3. For the 2H-TMDC materials, the Poisson ratio $\nu_\perp$ that governs out-of plane variation of h in response to an in-plane strain according to $\Delta h/h = -\nu_\perp(\varepsilon_{11} + \varepsilon_{22})$ is obtained directly from the relaxed structures. All calculated elastic coefficients satisfy the Born stability criteria for crystals possessing hexagonal symmetry.[27,39] The ab initio-calculated C_{11} and C_{12} values for monolayer h-BN and monolayer 2H-MoS2 are within approximately 10% of available elastic coefficients experimentally measured in the bulk phase, after converting the latter to a per-monolayer two-dimensional (2D) form.[40,41]

Table 3. Calculated Clamped-Ion and Relaxed-Ion Components, C_{11} and C_{12}, of the Elastic Tensor for Each Piezoelectric Monolayer at the DFT/GGA Level of Theory[a]

	clamped-ion		relaxed-ion		
material	C_{11} (N/m)	C_{12} (N/m)	C_{11} (N/m)	C_{12} (N/m)	$\nu_\perp$
h-BN	300	53	291	62	
2H-MoS_2	153	48	130	32	0.34
2H-$MoSe_2$	131	39	108	25	0.35
2H-$MoTe_2$	101	32	80	21	0.37
2H-WS_2	170	56	144	31	0.36
2H-WSe_2	147	40	119	22	0.36
2H-WTe_2	116	31	89	15	0.39

[a]The Poisson ratio $\nu_\perp$ that governs elastic relaxations in h is also calculated where relevant.

The linear piezoelectric effect in a flat and 2D material can be viewed as a first-order coupling between surface polarization (P_i) or the macroscopic electric field (E_i), and stress (σ_{jk}) or the strain (ε_{jk}) tensors, where i, j, $k \in \{1,2,3\}$, with 1, 2, and 3 corresponding to x, y, and z, respectively. The effect can be described using the third-rank piezoelectric tensors d_{ijk}, e_{ijk}, and their respective Maxwell relations:[27]

$$d_{ijk} = \left(\frac{\partial P_i}{\partial \sigma_{jk}}\right)_{E,T} = \left(\frac{\partial \varepsilon_{jk}}{\partial E_i}\right)_{\sigma,T} \tag{2}$$

$$e_{ijk} = \left(\frac{\partial P_i}{\partial \varepsilon_{jk}}\right)_{E,T} = -\left(\frac{\partial \sigma_{jk}}{\partial E_i}\right)_{\varepsilon,T} \tag{3}$$

It can be shown that d_{ijk} and e_{ijk} are related via the elastic stiffness tensor, C_{ijkl}. Both monolayers of h-BN and of 2H-TMDC belong to the D_{3h} ($\bar{6}m2$) point group. This symmetry places restrictions on the magnitude and uniqueness of the piezoelectric tensor coefficients. In the case of D_{3h}, only one d- and one e-coefficient need to be calculated. Employing Voigt notation to limit the number of indices, the only allowed nonzero piezoelectric d-coefficients are[27]

$$\begin{aligned} d_{111} &= d_{11} \\ d_{122} &= d_{12} = -d_{11} \\ d_{212} &= d_{221} = \frac{1}{2}d_{26} = -d_{11} \end{aligned} \tag{4}$$

Similar, but slightly different relations hold for the nonzero e-coefficients:

$$\begin{aligned} e_{111} &= e_{11} \\ e_{122} &= e_{12} = -e_{11} \\ e_{212} &= e_{221} = e_{26} = -e_{11} \end{aligned} \tag{5}$$

All in-plane elastic and piezoelectric properties of D_{3h} monolayers are fully determined by only three coefficients because d_{11} and e_{11} are related as follows:

$$e_{11} = d_{11}(C_{11} - C_{12}) \tag{6}$$

In order to complete the picture, we calculate the change in polarization along x per unit cell using the geometric phase approach of King-Smith and Vanderbilt[42,43] implemented in Quantum Espresso.[44] The clamped- and relaxed-ion piezoelectric e_{11}-coefficients are subsequently obtained by least-squares fitting of the polarization change per unit area to eq 7:

$$P_1(\varepsilon_{11}, \varepsilon_{22} = 0) - P_1(\varepsilon_{11} = 0, \varepsilon_{22} = 0) = e_{11}\varepsilon_{11} \quad (7)$$

Using eq 7, we calculate the relaxed-ion (clamped-ion) d_{11} by knowledge of the relaxed (clamped) results for e_{11}, C_{11} and C_{12}. Figure 2 illustrates the direct calculations of the piezoelectric e_{11}-coefficients and Table 4 gives the calculated d_{11} values. The calculated relaxed-ion d_{11}-coefficients, especially those for the 2H-TMDC monolayers, compare favorably with coefficients of frequently used bulk piezoelectrics such as α-quartz (d_{11} = 2.3 pm/V),[45] wurtzite GaN (d_{33} = 3.1 pm/V),[46] and wurtzite AlN (d_{33} = 5.1 pm/V).[46] The clamped-ion e_{11} coefficient for h-BN is in good agreement with the value of 3.57 × 10^{-10} C/m, calculated earlier by Naumov et al.[47] The entire range of calculated relaxed-ion d_{11}-coefficients spans more than 1 order of magnitude. Nevertheless, all the obtained relaxed-ion d_{11}- and e_{11}-coefficients *exceed* those predicted for e_{31}-/d_{31}-type engineered piezoelectricity in adatom-doped monolayer graphene,[20] and are generally 1 order of magnitude greater.

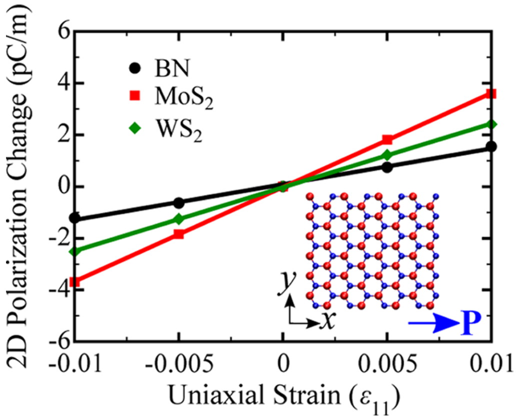

Figure 2. Applied uniaxial strain along the x-axis results in a change in polarization along the same axis for monolayer h-BN and MS_2 where M = Mo or W. Atom positions are relaxed under uniaxial strain to obtain the relaxed-ion piezoelectric coefficient determined by the slope of the line.

Table 4. Calculated Clamped-Ion and Relaxed-Ion Piezoelectric Coefficients, e_{11} and d_{11}[a]

	clamped-ion		relaxed-ion	
material	e_{11} (10^{-10} C/m)	d_{11} (pm/V)	e_{11} (10^{-10} C/m)	d_{11} (pm/V)
h-BN	3.71	1.50	1.38	0.60
2H-MoS_2	3.06	2.91	3.64	3.73
2H-$MoSe_2$	2.80	3.05	3.92	4.72
2H-$MoTe_2$	2.98	4.33	5.43	9.13
2H-WS_2	2.20	1.93	2.47	2.19
2H-WSe_2	1.93	1.80	2.71	2.79
2H-WTe_2	1.60	1.88	3.40	4.60
graphene + Li			0.15 (e_{31})[20]	0.55 (d_{31})[20]
bulk α-quartz				2.3 (d_{11})[45]
bulk GaN (wurtzite)				3.1 (d_{33})[46]
bulk AlN (wurtzite)				5.1 (d_{33})[46]

[a]Predicted 31-coefficients for piezoelectric lithium-doped monolayer graphene and experimentally measured d-coefficients of popular bulk piezoelectrics α-quartz, GaN, and AlN are listed for comparison.

We find that the relaxed-ion e_{11} and d_{11} coefficients in the 2H-TMDC monolayers obey a periodic trend. WS_2 possesses the smallest piezoelectric effect, and moving upward in group 6 (transition metal) or downward group 16 (chalcogenide) enhances the magnitude of the effect until $MoTe_2$, having the largest coefficient, is reached. The trend is more dramatic in d_{11} because there also are trends in C_{11} and C_{12} that serve to amplify the trend in e_{11}. Figure 3 summarizes all the periodic trends strictly obeyed by our data.

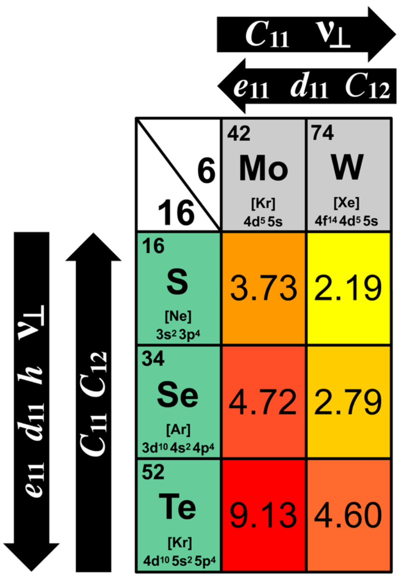

Figure 3. Trends in relaxed-ion structural, elastic, and piezoelectric properties of 2H-MX_2, where M = Mo or W, and X = S, Se, or Te. The relaxed-ion d_{11} coefficient values are listed as an example.

Here we have shown, for the first time, that many of the 2D materials at the center of considerable research focus are in fact piezoelectric. Because of its surprising magnitude, the piezoelectric effect in these 2D materials is much more than a theoretical curiosity. We are optimistic that this piezoelectric effect can be quantified in a relatively straightforward experiment on TMDC flakes. For example, because of transition metals' strong interaction with X-ray radiation, monolayer flakes may be utilized for precise measurement of field-induced strain. Conversely, experiments can be envisioned where an applied strain is directly correlated to a measurable voltage across a finite-size flake, turning the monolayer sheet into a highly sensitive strain gauge. We expect the piezoelectric properties of these materials to provide new platforms for electronic and piezotronic devices, and enable previously inaccessible avenues for sensing and control at the nanoscale.

■ COMPUTATIONAL METHODS

We used DFT implemented within the Quantum-ESPRESSO 5.0 ab initio software package.[44] Depending on the material simulated, ion cores were treated using ultrasoft Vanderbilt,[48] norm-conserving,[49] and projector augmented-wave[50] pseudopotentials, as listed in Table 1. Electron exchange and correlation effects were described using the generalized-gradient-corrected Perdew-Burke-Ernzerhof (PBE) approximation.[51] Periodic boundary conditions were employed in all three dimensions using an orthorhombic unit cell containing either two boron atoms and two nitrogen atoms for BN, or four chalcogenide atoms and two transition metal atoms for the TMDC systems. Note the hexagonal primitive cell was not used in order to align the direction of polarization along one of the lattice vectors (i.e., the x-axis). A 30 Å cell height was used in the z-direction to prevent periodic images from interacting with each other. The electronic wave function was expanded in a plane wave basis set with an energy cutoff of 60 Ry. The charge density was expanded in a basis set with a 500 Ry plane wave cutoff. Brillouin zone sampling was done using a Monkhorst-Pack mesh[52] of $14 \times 14 \times 1$ k-points. All ionic relaxations and cell optimizations were performed using a threshold of 10^{-4} Ry/Bohr for the force and 10^{-6} Ry for the unit cell energy.

■ AUTHOR INFORMATION

Corresponding Author

*E-mail: evanreed@stanford.edu; Tel: [+1] (650) 723 2971; Fax: [+1] (650) 725 4034.

Author Contributions

†These authors contributed equally to this work.

Notes

The authors declare no competing financial interest.

■ ACKNOWLEDGMENTS

Our work was supported in part by the U.S. Army Research Laboratory, through the Army High Performance Computing Research Center, Cooperative Agreement W911NF-07-0027. This work was also partially supported by DARPA YFA Grant N66001-12-1-4236, and used resources of the National Energy Research Scientific Computing Center (NERSC), which is supported by the Office of Science of the U.S. Department of Energy under Contract No. DE-AC02-05CH11231. Some calculations were performed in part using the Stanford NNIN Computing Facility (SNCF), a member of the National Nanotechnology Infrastructure Network (NNIN), supported by the National Science Foundation (NSF). The authors would like to thank Yao Li for helpful discussions and Dr. Tingting Qi for useful comments and for providing us with norm-conserving W and Mo pseudopotentials. We also acknowledge and recommend the online NNIN/C Pseudopotential Virtual Vault located at http://nninc.cnf.cornell.edu/.

■ REFERENCES

(1) Jensen, K.; Weldon, J.; Garcia, H.; Zettl, A. Nanotube Radio. *Nano Lett.* **2007**, *7*, 3508−3511.

(2) Lee, S. W.; Lee, D. S.; Morjan, R. E.; Jhang, S. H.; Sveningsson, M.; Nerushev, O. A.; Park, Y. W.; Campbell, E. E. B. A Three-Terminal Carbon Nanorelay. *Nano Lett.* **2004**, *4*, 2027−2030.

(3) Kaul, A. B.; Wong, E. W.; Epp, L.; Hunt, B. D. Electromechanical Carbon Nanotube Switches for High-Frequency Applications. *Nano Lett.* **2006**, *6*, 942−947.

(4) Standley, B.; Bao, W. Z.; Zhang, H.; Bruck, J.; Lau, C. N.; Bockrath, M. Graphene-Based Atomic-Scale Switches. *Nano Lett.* **2008**, *8*, 3345−3349.

(5) Kim, P.; Lieber, C. M. Nanotube Nanotweezers. *Science* **1999**, *286*, 2148−2150.

(6) Nishio, M.; Sawaya, S.; Akita, S.; Nakayama, Y. Carbon Nanotube Oscillators Toward Zeptogram Detection. *Appl. Phys. Lett.* **2005**, *86*, 133111.

(7) Arsat, R.; Breedon, M.; Shafiei, M.; Spizziri, P. G.; Gilje, S.; Kaner, R. B.; Kalantar-Zadeh, K.; Wlodarski, W. Graphene-like Nano-sheets for Surface Acoustic Wave Gas Sensor Applications. *Chem. Phys. Lett.* **2009**, *467*, 344−347.

(8) Stampfer, C.; Helbling, T.; Obergfell, D.; Schoberle, B.; Tripp, M. K.; Jungen, A.; Roth, S.; Bright, V. M.; Hierold, C. Fabrication of Single-Walled Carbon-Nanotube-Based Pressure Sensors. *Nano Lett.* **2006**, *6*, 233−237.

(9) Grow, R. J.; Wang, Q.; Cao, J.; Wang, D. W.; Dai, H. J. Piezoresistance of Carbon Nanotubes on Deformable Thin-Film Membranes. *Appl. Phys. Lett.* **2005**, *86*, 093104.

(10) Stampfer, C.; Jungen, A.; Linderman, R.; Obergfell, D.; Roth, S.; Hierold, C. Nano-electromechanical Displacement Sensing Based on Single-Walled Carbon Nanotubes. *Nano Lett.* **2006**, *6*, 1449−1453.

(11) Tans, S. J.; Verschueren, A. R. M.; Dekker, C. Room-Temperature Transistor Based on a Single Carbon Nanotube. *Nature* **1998**, *393*, 49−52.

(12) Li, X.; Wang, X.; Zhang, L.; Lee, S.; Dai, H. Chemically Derived, Ultrasmooth Graphene Nanoribbon Semiconductors. *Science* **2008**, *319*, 1229−1232.

(13) Radisavljevic, B.; Radenovic, A.; Brivio, J.; Giacometti, V.; Kis, A. Single-Layer MoS_2 Transistors. *Nat. Nanotechnol.* **2011**, *6*, 147−150.

(14) Yang, Q.; Wang, W.; Xu, S.; Wang, Z. L. Enhancing Light Emission of ZnO Microwire-Based Diodes by Piezo-Phototronic Effect. *Nano Lett.* **2011**, *11*, 4012−4017.

(15) Qin, Y.; Wang, X.; Wang, Z. L. Microfibre-Nanowire Hybrid Structure for Energy Scavenging. *Nature* **2008**, *451*, 809−813.

(16) Wang, Z. L.; Song, J. Piezoelectric Nanogenerators Based on Zinc Oxide Nanowire Arrays. *Science* **2006**, *312*, 242−246.

(17) Bykhovski, A.; Gelmont, B.; Shur, M. The Influence of the Strain-Induced Electric Field on the Charge Distribution in GaN-AlN-GaN Structure. *J. Appl. Phys.* **1993**, *74*, 6734.

(18) Proie, R. M.; Polcawich, R. G.; Pulskamp, J. S.; Ivanov, T.; Zaghloul, M. E. Development of a PZT MEMS Switch Architecture for Low-Power Digital Applications. *J. MEMS* **2011**, *20*, 1032−1042.

(19) Wang, Z. L. Nanopiezotronics. *Adv. Mater.* **2007**, *19*, 889−892.

(20) Ong, M. T.; Reed, E. J. Engineered Piezoelectricity in Graphene. *ACS Nano* **2012**, *6*, 1387−1394.

(21) Chandratre, S.; Sharma, P. Coaxing Graphene to be Piezo-electric. *Appl. Phys. Lett.* **2012**, *100*, 023114.

(22) Novoselov, K. S.; Jiang, D.; Schedin, F.; Booth, T. J.; Khotkevich, V. V.; Morozov, S. V.; Geim, A. K. Two-Dimensional Atomic Crystals. *Proc. Natl. Acad. Sci. U.S.A.* **2005**, *102*, 10451−10453.

(23) This notation is lacking in the case of monolayers because the 2H prefix provides insufficient information about in-plane structure to differentiate from octahedrally coordinated TMDCs. The 2 is, of course, irrelevant in the monolayer case. In this article, however, we take 2H to denote monolayers with trigonal prismatic coordination for the sake of consistency.

(24) Joensen, P.; Frindt, R. F.; Morrison, S. R. Single-Layer MoS_2. *Mater. Res. Bull.* **1986**, *21*, 457−461.

(25) Yang, D.; Frindt, R. F. Li-Intercalation and Exfoliation of WS_2. *J. Phys. Chem. Solids* **1996**, *57*, 1113−1116.

(26) Coleman, J. N.; Lotya, M.; O'Neill, A.; Bergin, S. D.; King, P. J.; Khan, U.; Young, K.; Gaucher, A.; De, S.; Smith, R. J.; et al. Two-Dimensional Nanosheets Produced by Liquid Exfoliation of Layered Materials. *Science* **2011**, *331*, 568−571.

(27) Nye, J. F. *Physical Properties of Crystals: Their Representation by Tensors and Matrices*; Clarendon Press: Oxford, U.K., 1957.

(28) Pease, R. S. An X-Ray Study of Boron Nitride. *Acta Crystallogr.* **1952**, *5*, 356−361.

(29) Wilson, J. A.; Yoffe, A. D. Transition Metal Dichalcogenides Discussion and Interpretation of Observed Optical, Electrical and Structural Properties. *Adv. Phys.* **1969**, *18*, 193−335.

(30) Nakhmanson, S.; Calzolari, A.; Meunier, V.; Bernholc, J.; Buongiorno Nardelli, M. Spontaneous Polarization and Piezoelectricity in Boron Nitride Nanotubes. *Phys. Rev. B* **2003**, *67*, 235406.

(31) Shimada, K. First-Principles Determination of Piezoelectric Stress and Strain Constants of Wurtzite III-V Nitrides. *Jpn. J. Appl. Phys.* **2006**, *45*, L358−L360.

(32) Opium - pseudopotential generation project at http://opium.sourceforge.net.

(33) Fang, H.; Chuang, S.; Chang, T. C.; Takei, K.; Takahashi, T.; Javey, A. High-Performance Single Layered WSe_2 p-FETs with Chemically Doped Contacts. *Nano Lett.* **2012**, *12*, 3788−3792.

(34) Mak, K.; Lee, C.; Hone, J.; Shan, J.; Heinz, T. Atomically Thin MoS_2: A New Direct-Gap Semiconductor. *Phys. Rev. Lett.* **2010**, 105.

(35) Yang, D.; Sandoval, S.; Divigalpitiya, W.; Irwin, J.; Frindt, R. Structure of Single-Molecular-Layer MoS_2. *Phys. Rev. B* **1991**, *43*, 12053−12056.

(36) Gordon, R. A.; Yang, D.; Crozier, E. D.; Jiang, D. T.; Frindt, R. F. Structures of Exfoliated Single Layers of WS_2, MoS_2, and $MoSe_2$ in Aqueous Suspension. *Phys. Rev. B* **2002**, *65*, 1254071−1254079.

(37) Lee, C.; Yan, H.; Brus, L. E.; Heinz, T. F.; Hone, J.; Ryu, S. Anomalous Lattice Vibrations of Single- and Few-Layer MoS_2. *ACS Nano* **2010**, *4*, 2695−2700.

(38) Brown, B. E. The Crystal Structures of WTe_2 and High-Temperature $MoTe_2$. *Acta Crystallogr.* **1966**, *20*, 268−274.

(39) Born, M.; Huang, K. *Dynamical Theory of Crystal Lattices*; Oxford University Press: Oxford, U.K., 1988.

(40) Feldman, J. L. Elastic-Constants of 2H-MoS_2 and 2H-$NbSe_2$ Extracted from Measured Dispersion Curves and Linear Compressibilities. *J. Phys. Chem. Solids* **1976**, *37*, 1141−1144.

(41) Bosak, A.; Serrano, J.; Krisch, M.; Watanabe, K.; Taniguchi, T.; Kanda, H. Elasticity of Hexagonal Boron Nitride: Inelastic X-ray Scattering Measurements. *Phys. Rev. B* **2006**, *73*, 041402.

(42) King-Smith, R. D.; Vanderbilt, D. Theory of Polarization of Crystalline Solids. *Phys. Rev. B* **1993**, *47*, 1651−1654.

(43) Resta, R.; Vanderbilt, D. *Physics of Ferroelectrics: A Modern Perspective*; Springer-Verlag: Berlin, 2007; pp 31−68.

(44) Giannozzi, P.; Baroni, S.; Bonini, N.; Calandra, M.; Car, R.; Cavazzoni, C.; Ceresoli, D.; Chiarotti, G. L.; Cococcioni, M.; Dabo, I.; et al. QUANTUM ESPRESSO: A Modular and Open-Source Software Project for Quantum Simulations of Materials. *J. Phys.: Condens. Matter* **2009**, *21*, 395502.

(45) Bechmann, R. Elastic and Piezoelectric Constants of Alpha-Quartz. *Phys. Rev.* **1958**, *110*, 1060−1061.

(46) Lueng, C. M.; Chan, H. L. W.; Surya, C.; Choy, C. L. Piezoelectric Coefficient of Aluminum Nitride and Gallium Nitride. *J. Appl. Phys.* **2000**, *88*, 5360.

(47) Naumov, I.; Bratkovsky, A. M.; Ranjan, V. Unusual Flexoelectric Effect in Two-Dimensional Noncentrosymmetric sp^2-Bonded Crystals. *Phys. Rev. Lett.* **2009**, *102*, 217601.

(48) Vanderbilt, D. Soft Self-Consistent Pseudopotentials in a Generalized Eigenvalue Formalism. *Phys. Rev. B* **1990**, *41*, 7892−7895.

(49) Troullier, N.; Martins, J. L. Efficient Pseudopotentials for Plane-Wave Calculations. *Phys. Rev. B* **1991**, *43*, 1993−2006.

(50) Blochl, P. E. Projector Augmented-Wave Method. *Phys. Rev. B* **1994**, *50*, 17953−17979.

(51) Perdew, J. P.; Burke, K.; Ernzerhof, M. Generalized Gradient Approximation Made Simple. *Phys. Rev. Lett.* **1996**, *77*, 3865−3868.

(52) Monkhorst, H. J.; Pack, J. D. Special Points for Brillouin-Zone Integrations. *Phys. Rev. B* **1976**, *13*, 5188−5192.